JOURNAL OF PROPULSION AND POWER
Vol. 10, No. 4, July–Aug. 1994

Direct Simulation Monte Carlo Model of Low Reynolds Number Nozzle Flows

Donna Zelesnik,* Michael M. Micci,† and Lyle N. Long‡
Pennsylvania State University, University Park, Pennsylvania 16802

A numerical analysis of low Reynolds number nozzle flows is performed to investigate the loss mechanisms involved and to determine the nozzle wall contour that minimizes these losses. The direct simulation Monte Carlo method is used to simulate nitrogen flows through conical, trumpet-shaped, and bell-shaped nozzles at inlet stagnation temperatures of 300 and 1000 K. The Reynolds number of the flows based on throat diameter range from 90 to 125. The trumpet-shaped nozzle has the highest efficiency with the unheated flow. With the heated flow both the trumpet and bell-shaped nozzles have a 6.5% higher efficiency than the conical nozzle. The conical nozzle has the highest discharge coefficient, which is unaffected by the change in stagnation temperature; however, the increase in stagnation temperature increases the heat-transfer and viscous losses in the boundary layer. These results suggest that the trumpet-shaped wall contour performs most efficiently except near the throat region, where it incurs large viscous losses. However, the bell-shaped nozzle may increase its overall performance with an increase in stagnation temperature.

Introduction

THE significant limiting factor in satellite lifetime is the ability of its propulsion system to efficiently utilize the available energy in the onboard propellant for stationkeeping and orbital maneuvering. In response to this limitation, intense research has been conducted to optimize the performance of the small, high-performance chemical rocket motors and electrothermal propulsion devices used on these spacecraft. The low-thrust rocket engines produce levels of thrust on the order of tenths of Newtons and are highly inefficient systems. One area in which considerable improvement can be made is in nozzle efficiency, because high nozzle losses are suffered due to the low Reynolds number of the exhaust flow.

The combination of small size and low-density flow leads to very low Reynolds numbers, ranging from 10^2 to 10^3 based on throat diameter. The Reynolds number, with the throat diameter as the characteristic dimension, is given by the relation

$$Re = (\rho U D_t/\mu) \tag{1}$$

where ρ is the flow density, U is the axial velocity component, D_t is the nozzle throat diameter, and μ is the coefficient of viscosity. The major consequence of low Reynolds number flow is rapid boundary-layer growth within the nozzle diffuser. This boundary layer fills most, if not all, of the throat and divergent nozzle section. When this occurs, there is no distinction between an inner viscous layer and an outer layer of potential flow. The term "boundary layer" may be inappropriate in this case, and so the term "viscous layer" is used instead to describe the nozzle flow. A great deal of energy in the form of heat is lost to the viscous layer through viscous dissipation, which has a dire effect on thrust and efficiency by causing the flow temperature to rise. In a low Reynolds number nozzle, much of the thermal energy is not converted to velocity due to heating in the viscous layer. At very low Reynolds numbers, the flow temperature may actually increase after an initial decrease if the viscous layer grows to fill the entire nozzle.

Nozzle efficiency η_{isp}, is measured by the ratio of the delivered specific impulse to the ideal specific impulse predicted by one-dimensional isentropic gas dynamic relations

$$\eta_{isp} = (Isp_{\text{actual}}/Isp_{\text{ideal}}) \tag{2}$$

where the equation for specific impulse Isp is:

$$Isp = (I/M_P g_e) = (U_{eq}/g_e) \tag{3}$$

and I is the total impulse, M_p is the total propellant mass expelled, and g_e is the gravitational constant. Nozzle efficiency decreases rapidly as throat Reynolds number decreases, and has been measured as low as 75% at a Reynolds number of 500.[1]

The Reynolds number is proportional to nozzle throat diameter and inversely proportional to stagnation temperature

$$Re \propto (P_0 D_t/T_0) \tag{4}$$

and therefore the Reynolds number decreases as throat diameter decreases or as the chamber stagnation temperature increases. As both chemical and electrothermal thruster research and development strive for higher chamber temperatures to increase performance, the future trend for spacecraft thrusters will be for decreasing nozzle Reynolds numbers. The need exists for a better understanding of the flow mechanisms involved in order to offset the effects of low Reynolds number flow and increase the efficiency of low-thrust rocket motors.

The majority of past efforts to increase nozzle efficiency have been trial and error iterations on the diffuser geometry, or wall contour. Experimental measurements have consisted of thrust and discharge coefficient, both global quantities which give little information about the detailed physical processes occurring within the nozzle. Different studies looking for the optimal nozzle wall contour for low Reynolds number flow among cones of various angles, bell- and trumpet-shaped nozzles reached different conclusions. Results also varied between ambient and elevated temperature gas flows and between gases with different compositions.[1-3] The only detailed

Received Nov. 25, 1992; revision received Nov. 22, 1993; accepted for publication Nov. 22, 1993.

*Graduate Student, Department of Aerospace Engineering. Student Member AIAA.

†Associate Professor, Department of Aerospace Engineering. Member AIAA.

‡Assistant Professor, Department of Aerospace Engineering. Member AIAA.

measurements of flow properties within low Reynolds number conical nozzles were taken by Rothe[4] using an electron beam diagnostic in a low-pressure nozzle flow. Rothe measured density and temperature as a function of axial and radial location in the expansion region of the nozzle and found that for low flow Reynolds numbers the static temperature rises in the nozzle expansion due to viscous dissipation, and that the effect becomes more pronounced as the nozzle Reynolds number decreases. A study of low-density nozzle flows in the exit plane and plume was carried out by Penko et al.[5] Penko measured radial pitot pressure profiles at different axial locations in the plume and compared the experimental results with numerical calculations. He found good agreement between the data and the numerical results.

Prior to the advent of molecular gas dynamics models and the increase in supercomputing efficiency, past computational efforts for the estimation of rocket nozzle performance were based on the assumption that the flow could be subdivided into an inviscid core and a classical boundary layer. Numerical solutions utilized approximations to the full Navier-Stokes equations, such as the classical boundary-layer equations and the slender channel approximations.[6] Other methods, including equilibrium method of characteristics solutions, have been used in the nozzle design process.[7] Simple formulas based on both analytic approaches and empirical data have been obtained to predict performance characteristics such as nozzle discharge coefficient as a function of Reynolds number.[8]

All of these methods rely on assumptions that are not entirely accurate, the most significant of which is that the Navier-Stokes equations are even applicable to this type of flow. The Knudsen number Kn defined as the ratio between the mean free path λ and a characteristic flow dimension, determines the limit of applicability of the continuum flow equations. It is sometimes referred to as the degree of flow rarefaction. As the Knudsen number becomes greater than 0.1, the flow begins to transition to free molecular, where it is essentially collisionless, and the continuum equations are no longer strictly valid.[9] When the throat Reynolds number in low-density nozzles is on the order of 100, the flow becomes highly rarefied downstream from the throat in the nozzle expansion region. With the local nozzle diameter as the characteristic dimension, the Knudsen number progresses from approximately 0.02 at the throat to greater than 0.2 at the exit plane, and even higher in the plume, as calculated for a typical arcjet nozzle flow. Thus, the Navier-Stokes equations do not apply to the entire nozzle flowfield, but were used in the past as the best approximations available.

The direct simulation Monte Carlo (DSMC) method pioneered by Bird[9] is based on kinetic theory and is applicable to all three types of flows: 1) continuum, 2) transitional, and 3) free molecular. It is not practical in the continuum regime, however, due to the computational requirements. Because the Boltzmann equation can be derived from Bird's collisional scheme, the same assumptions are made for both DSMC and the Boltzmann equation. This method has been utilized recently to simulate low Reynolds number nozzle flows, particularly to investigate plume backflow. Campbell[10] investigated the detailed flow structure in the region near the lip of a nozzle flowing to vacuum with Bird's DSMC technique. He made comparisons of the plume flowfield predictions with experimental measurements and verified the nonequilibrium nature of the flow. Hueser et al.[7] also used DSMC to study flow around the nozzle lip and found large differences between the DSMC predictions and those of the equilibrium method of characteristics solutions, as would be expected.

The exhaust gas flow of the bipropellant engine for the Mars Observer Scientific Spacecraft was simulated with DSMC by Ratterni.[11] The results were used to determine the effects of plume heating and impingement on the spacecraft. Nelson and Doo[12] simulated multicomponent nozzle flows of a 22-N rocket thruster into a vacuum with the Monte Carlo method. They found excellent agreement with existing experimental mass flux data. Boyd and Stark[13] modeled small hydrazine thruster plumes to compare continuum methods with DSMC predictions, and concluded that the DSMC method is the proper technique to be used to investigate low-density nozzle exhaust plumes. Boyd et al.[14] compared experimental pitot pressure data with predictions obtained by both continuum methods and DSMC, and also concluded that the DSMC results matched the experimental data more closely than the continuum results.

In this study, DSMC is used to simulate the flow in the divergent nozzle section, with the input conditions obtained from numerical continuum calculations in the nozzle inlet. The viscous layer growth and changes in temperature and pressure, as well as overall performance characteristics are studied in order to gain a better understanding of the flow phenomena. Most importantly, this research concentrates on the determination of the optimal nozzle wall contour for both heated and unheated nitrogen flows.

Direct Simulation Monte Carlo Method

The DSMC technique utilizes a small number of simulated particles in a region of space to represent real molecules in physical space and time. Each simulated molecule represents a specific, much larger number of actual molecules. The ratio of real to simulated molecules depends on flow density and computational grid size. The molecules advance in space and are taken through representative collisions, chemical reactions, and boundary interactions. Each molecule's position coordinates, velocity components, and internal states are stored and modified with time.

The simulated region is divided into cells for both sampling purposes and for the selection of collision pairs. Bird's time counter method[15] is the algorithm used to select collision pairs and calculate the collisions. Two time steps are used to increment time: 1) global flow time and 2) cell collision time. Global flow time is incremented in the molecular motion stage where the particles advance in space based on their individual velocities without interaction with other particles. Collision partners are then chosen in each cell. The number of collisions per cell varies from cell to cell, and depends on the mean collision time and the relative velocity of the colliding molecules. When a collision occurs in the cell, the collision time is incremented. After a number of collisions have occurred, the total collision time increases until it exceeds the global flow time limit. Hence, the number of collisions per cell is not predetermined. In each cell, the molecules are selected for collisions on a probabilistic basis, so no flow gradients can occur across a cell, only from cell to cell. Because the mean collision time and mean free path vary spatially, both the time step and cell size vary from region to region in the simulated physical space.

The most important assumption of this technique is that the movement of the molecules can be decoupled from the collisions. To validate this assumption, the time step must be small in comparison to the mean collision time. In addition, the cell dimensions must be small in comparison with the local mean free path λ. The recommended maximum value for cell size[9] is $\lambda/3$. A necessary requirement for general numerical accuracy is that there are enough grid points to capture the local flow gradients. For example, the cell dimension should be much less than $\phi/\nabla\phi$, where ϕ is any suitable macroscopic property and ∇ is the gradient operator.

Steady state occurs when approximately the same number of molecules enter and exit the simulated region, at which time sampling of the macroscopic flow properties begins. The samples are determined by recording the positions and velocities of each molecule relative to the cell boundaries. Statistical scatter decreases as the square root of the sample size, and therefore a minimum sample size of 10,000 samples per cell is required to have less than a 1% statistical distribution.[9]

The variable hard sphere (VHS) gas model[16] is used in this study, and is capable of modeling the temperature depen-

dence of the viscosity of real molecules. The nozzle wall is modeled as a thermally accommodating surface boundary with fully diffuse reflections. This condition is equivalent to specifying a no-slip viscous boundary condition for very small Knudsen numbers, because the reflected velocity of each molecule is independent of its incident velocity. The reflected velocity distribution is instead dependent on the wall temperature and thermal accommodation.

In order to model the energy transfer between internal and translational energy modes, the Larson-Borgnakke model[17] is used. In this model, a fraction of the collisions are regarded as elastic and are calculated as if the gas is monatomic. The other fraction of collisions are treated as inelastic, and energy is transferred between translational and rotational energy modes based on the distributions of these quantities for an equilibrium gas. The fraction of inelastic collisions is a constant based on the real gas rotational relaxation rate.

Numerical Modeling of Nozzle Flow

The computational grid represents an axisymmetric slice through the divergent nozzle section and plume expansion area. The cell structure used to model the conical nozzle is shown in Fig. 1. The grid consists of 2500 cells, with the cell size varying according to gradients in the flow as well as local Knudsen number. All cells are smaller than the local mean free path. At the wall, where gradients are steepest, the cell-dimensions in the radial direction are very small as compared to the local characteristic lengths of the gradients. For example, the cell heights are two orders of magnitude smaller than $T/\nabla T$ and $\rho_n/\nabla\rho_n$, where T is temperature and ρ_n is number density, and one order of magnitude smaller than $U/\nabla U$, where U is axial velocity.

The flow is modeled by introducing molecules at the entrance to the simulated region and advancing them downstream. Note that the computational grid does not begin at the origin, which is the location of the nozzle throat, but begins instead downstream. Because the flow density in the supersonic region of the nozzle is highest near the throat, the local mean free path, and thus the necessary cell size, is very small in that region. The required number of cells to model this portion of the diffuser with the DSMC method is beyond the limits of the computational facilities available for this research, which consisted of an IBM 3090-600S mainframe and an IBM RS/6000 workstation. Therefore, a full Navier-Stokes code was used to solve the inlet nozzle flow.[18,19] This code solves the axisymmetric flow in a nozzle in a generalized coordinate system for subsonic and supersonic flows with characteristic boundary conditions. The Knudsen numbers at the cutoff point of the continuum code are within the continuum range of applicability, approximately $Kn = 0.02$. The continuum results are then used to specify the initial flow conditions for the DSMC analysis.

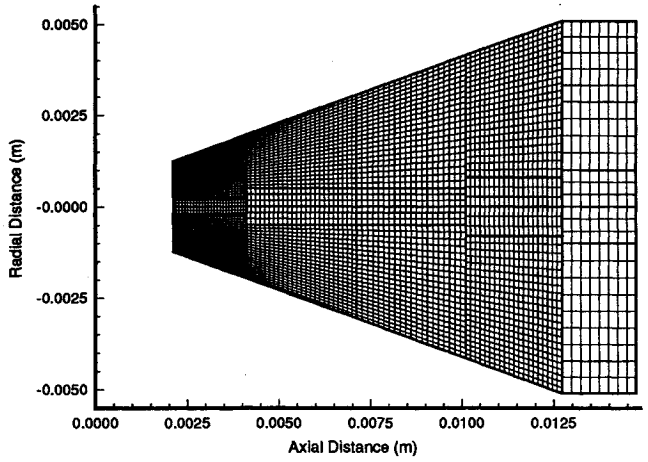

Fig. 1 Conical nozzle grid.

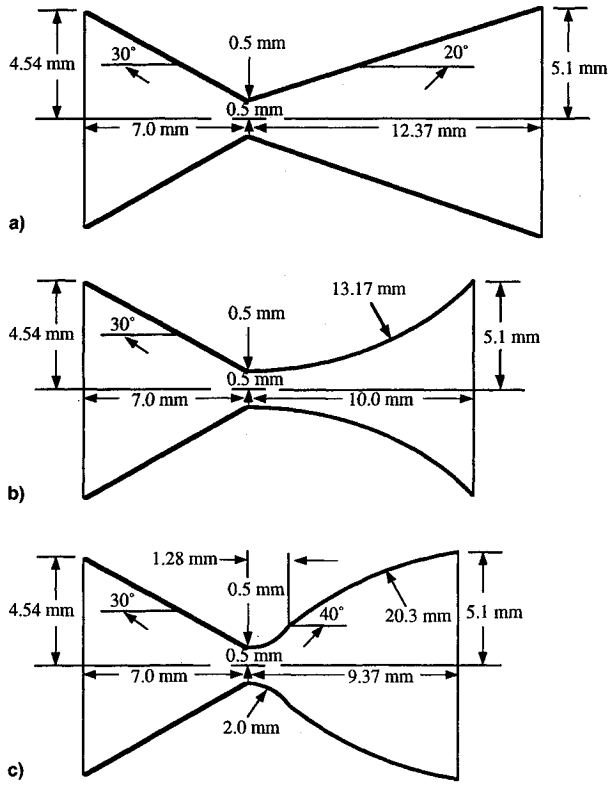

Fig. 2 Diagrams of nozzle geometries: a) cone, b) trumpet, and c) bell.

The wall is modeled as a constant temperature surface boundary at 293 K, and the exit plane and surrounding boundaries are modeled either as a pure vacuum or with a specified background density and temperature, depending on whether the conditions represent outer space or an experimental vacuum chamber. Once the number of molecules within the nozzle is constant, the flow becomes steady and sampling begins. Approximately 25–30 molecules per cell are present at steady state.

Nozzle Geometries and Flow Conditions

All three nozzle geometries modeled in this investigation have the identical inlet section and same expansion ratio, equal to 104. They only differ in the diffuser wall contour and the diffuser length. The wall contours were modeled after the experimental nozzles used by Grisnik and Smith.[1] Diagrams for each nozzle are shown in Fig. 2.

The inlet flow conditions are identical for all three geometries, and only differ for the unheated vs heated flow cases. The stagnation temperature for the unheated cases is 300 K, and equals 1000 K for the heated cases. The stagnation pressure is 1109.6 Pa. The throat Reynolds numbers for each case based on the inlet stagnation conditions are approximately $Re = 117$ for the unheated flows and $Re = 90$ for the heated flows.

The overall simulation consists of running six cases to investigate the flow of both heated and unheated nitrogen through the three different nozzle geometries. In addition to the individual flow properties such as density, pressure, Mach number, etc., six performance characteristics are examined and compared for each case. They include nozzle efficiency, discharge coefficient, thrust, specific impulse, viscous layer growth, and plume expansion.

Results and Discussion

DSMC Verification

In this section, pitot pressure measurements made by Penko et al.[5] at the exit plane and downstream of a low-density nozzle are presented and compared with DSMC results. A nu-

merical simulation of Penko's experiment was performed by Boyd et al.[20] in order to compare a vectorized version of Bird's particle method with the experimental data. The DSMC results from this investigation are compared with the DSMC predictions of Boyd as well as Penko's experimental data in order to validate the use of the DSMC method to investigate the performance of low-Reynolds number nozzles.

Two separate simulations were performed for the purpose of code validation using two different grids, with all other conditions remaining constant. The first grid contained 2254 cells, with 600 cells located in the region near the throat. Tens of thousands of samples were collected, but because the cell dimensions nearest the throat were approximately 50 times the local mean free path λ this grid was too coarse to accurately model the flow. The cell dimensions in the regions downstream of the throat were well within the limit of $\lambda/3$, due to the significant density decrease as the gas expands. The second grid contained 7250 cells, with 4550 cells in the region close to the throat. The addition of cells effectively reduced the cell sizes in that location to approximately 10λ, which was still too large, but the grid could not be made any finer due to computational limitations of the available facilities. In the simulation that used the finer grid, the total number of molecules present at steady state was approximately 175,000, which required a great deal of CPU time to perform the calculations. Less than half the number of samples were accumulated in the same amount of time it took with the coarser grid. The major difficulty encountered in the simulation of this particular nozzle flow study was the fact that the computations were begun exactly at the throat, where the gas is most dense, instead of further downstream, where the density has decreased significantly.

The calculated pitot pressure results at the exit plane using both grids are shown in Fig. 3 along with the experimental data and Boyd's DSMC results. The measurements begin at the nozzle axis and proceed radially towards the nozzle wall. All four plots have similar profiles, however, the DSMC results from this study underpredict the pressure close to the nozzle centerline. The use of the finer grid caused the results to move closer to the experimental data near the axis, but the results are still lower than both the experimental data and Boyd's DSMC results. The predictions from the simulation with the coarse grid compare well with the measurements at locations further away from the axis, and compare better than the results with the fine grid. More samples were taken with the coarse grid than could be accumulated with the fine grid, and since both grids were within the acceptable size range downstream of the throat, the larger number of samples may account for this difference.

A number of factors contribute to the differences between the DSMC results in this investigation and the numerical and experimental results of Boyd and Penko. Boyd used a highly vectorized version of Bird's DSMC code, and thus was able to use a grid containing 38,000 cells, all of which had a maximum dimension smaller than one mean free path. His computational domain employed 1.7 million particles. In comparison, the finest grid used in this investigation contained only 7250 cells and 175,000 molecules. Therefore, any error that was initiated at or near the throat, where the cells were the largest with respect to the local mean free path, propagated downstream and was magnified by the time it reached the exit plane and plume region. Another problem that was discovered late in the validation process was that the number of molecules in the cells near the centerline was significantly lower than in the cells closer to the wall. This also contributed to the error close to the nozzle centerline.

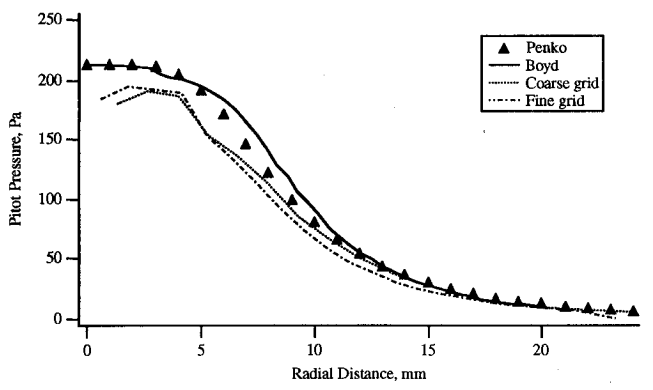

Fig. 3 Comparisons of computed and measured pitot pressure profiles at exit plane.

Two approximations were made in the physical modeling of the nozzle flow. First, it was assumed that the background was a perfect vacuum, while in the experiment a back pressure of 0.02 Pa was present. This assumption may explain why the DSMC predicted pressures were lower than the experimental results. The second assumption consisted of specifying a constant temperature at two locations on the nozzle wall instead of using the measured wall temperature profile. This approximation may have affected the results by improperly modeling the heat transfer to the fluid from the wall.

Overall, the DSMC results in this study compare fairly well with the experimental and numerical results of Boyd and Penko. It is expected that if the grid contained more and smaller computational cells, and if a minimum of 20 molecules were contained in each cell, the numerical results would be very similar to those of Boyd, and would compare very well with the experimental data. Care was taken in the remainder of the research that the above requirements were met.

Low Reynolds Number Nozzle Flow Simulations

A portion of the results of two sets of low Reynolds number nozzle flow simulations are presented for both unheated and heated nitrogen flows. For a complete discussion of the results, see Ref. 21. Six performance characteristics are compared in order to study the various loss mechanisms that occur in low Reynolds number nozzle flow, which include specific impulse efficiency, nozzle discharge coefficient, thrust output, specific impulse, viscous layer growth, and plume expansion. With the proper selection of nozzle geometry, these losses can be minimized.

Isograms of various flow properties are presented in Figs. 4–7, with all dimensions shown in meters. Thrust is computed by integrating the exit properties over the exit plane area. The flow is assumed to be a perfect gas, and so the perfect gas law is used to calculate pressure from density and temperature, where the gas constant for nitrogen at standard conditions is $R = 296$ J/(kg-s) and is constant for all flow conditions studied.

The discharge coefficient is the ratio of the actual mass flow rate to the theoretical maximum flow rate given by one-dimensional isentropic nozzle flow theory. In the present study, the ideal mass flow rate is calculated by integrating the mass flow as a function of stagnation pressure and temperature, P_0 and T_0, respectively, over the nozzle throat area. Both stagnation properties vary axially and radially due to viscous losses and heat transfer at the wall. Therefore, for the heated flow, the ideal mass flow rate is higher than the value calculated for constant inlet stagnation properties. It would be expected that since the inlet conditions and geometries are identical for all of the cases, the ideal mass flow rates would be equal for each set of unheated and heated flow cases. This is not the case, however, because the boundary layer at the throat is so large in each case. The flow in the boundary layer, which extends well into the diffuser, is subsonic for the most part. Since each geometry has a different diffuser wall contour beginning at the geometric throat, information propagates upstream in the subsonic boundary layer and causes the flow properties to be different at the throat for each case. In addition, the sonic throat, which is the location of the sonic line, is further downstream from the geometric throat in each case,

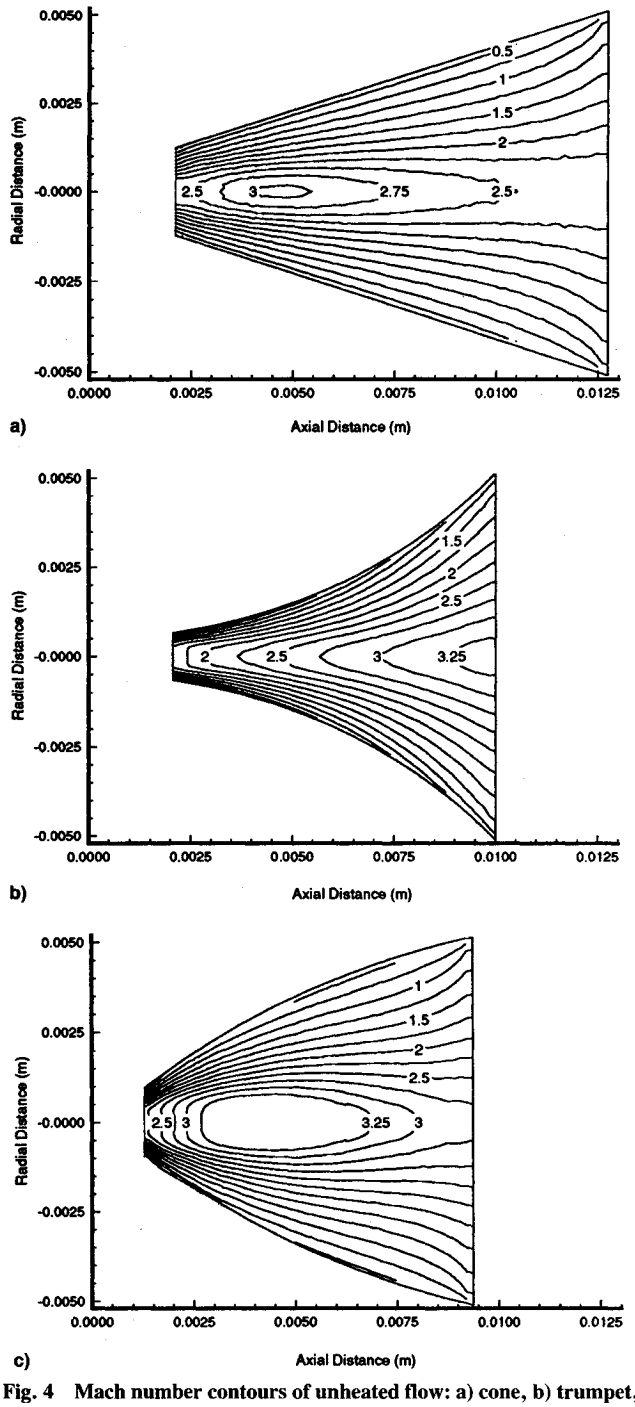

Fig. 4 Mach number contours of unheated flow: a) cone, b) trumpet, and c) bell.

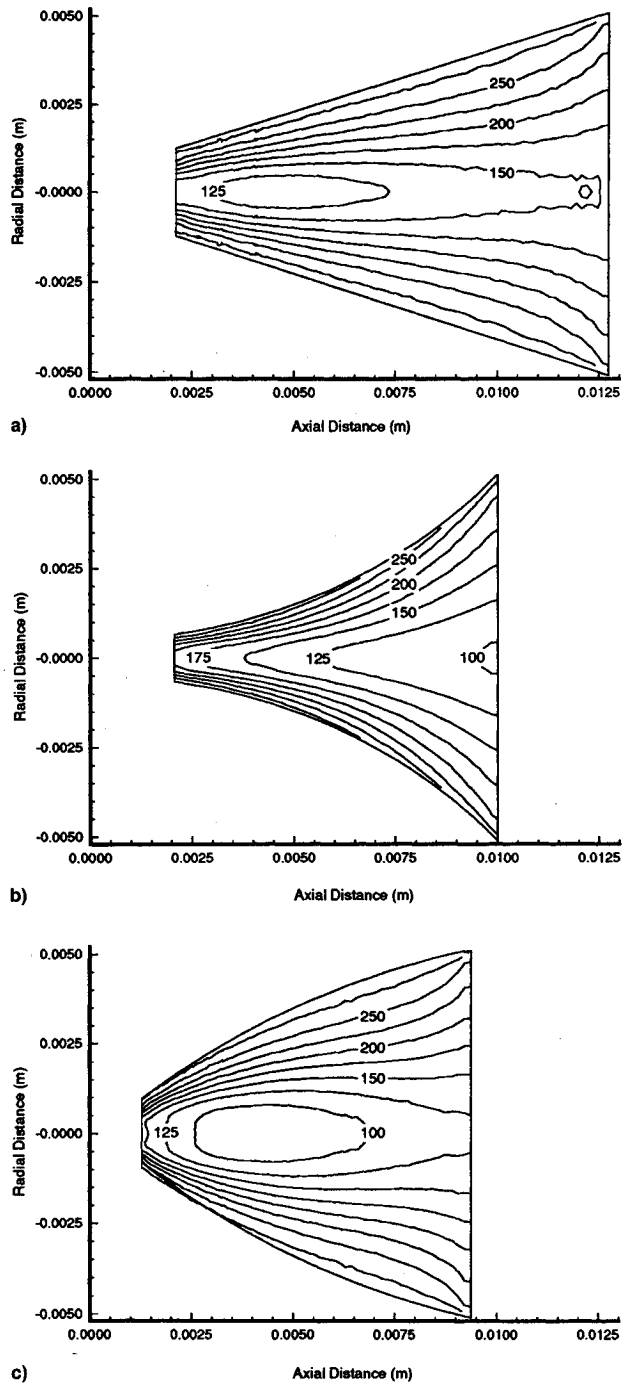

Fig. 5 Temperature contours of unheated flow (K): a) cone, b) trumpet, and c) bell.

and varies between geometries. The discharge coefficient is then calculated as the ratio between the actual mass flow rate, calculated at the exit plane, and the ideal mass flow rate, calculated at the nozzle throat.

Unheated Flow Results

In this section, the results from the unheated flow simulations are presented and compared. Figure 4 compares the Mach number contours plotted for each nozzle configuration. The most significant difference in results between the nozzles is that in both the cone and bell-shaped nozzles, the viscous layer grows to the point where it completely fills the nozzle well before the exit plane. In contrast, the flow expands closer to ideal in the trumpet-shaped nozzle. Although the flow expands to approximately a 16% higher Mach number in the bell-shaped nozzle, the region of high Mach number exists only at the very center of the diffuser. The flow recompresses in both the cone and bell-shaped nozzles, such that the average exit Mach number is equal to 2.5 or less. The Mach number at the trumpet-shaped nozzle exit is equal to 3.5 at the centerline and decreases to 1.5 at the wall.

Figure 5 depicts the temperature contour plots of each nozzle. The contour shapes are very similar to the Mach number contours, but the heat transfer in the viscous layer is more apparent with the temperature contours. The cone and bell-shaped nozzles appear to have thinner thermal boundary layers nearer the throat. At a location $x = 0.002$-m downstream of the throat, the trumpet-shaped nozzle flow is warmer than in the other two nozzles, but its viscous layer does not grow to the same extent as in the other two shapes. In addition to the heat transferred from the nozzle wall, a great deal of heat is generated in the viscous layer from viscous dissipation, causing the gas temperature to rise. Because the trumpet has a thinner viscous layer, the gas temperature decreases con-

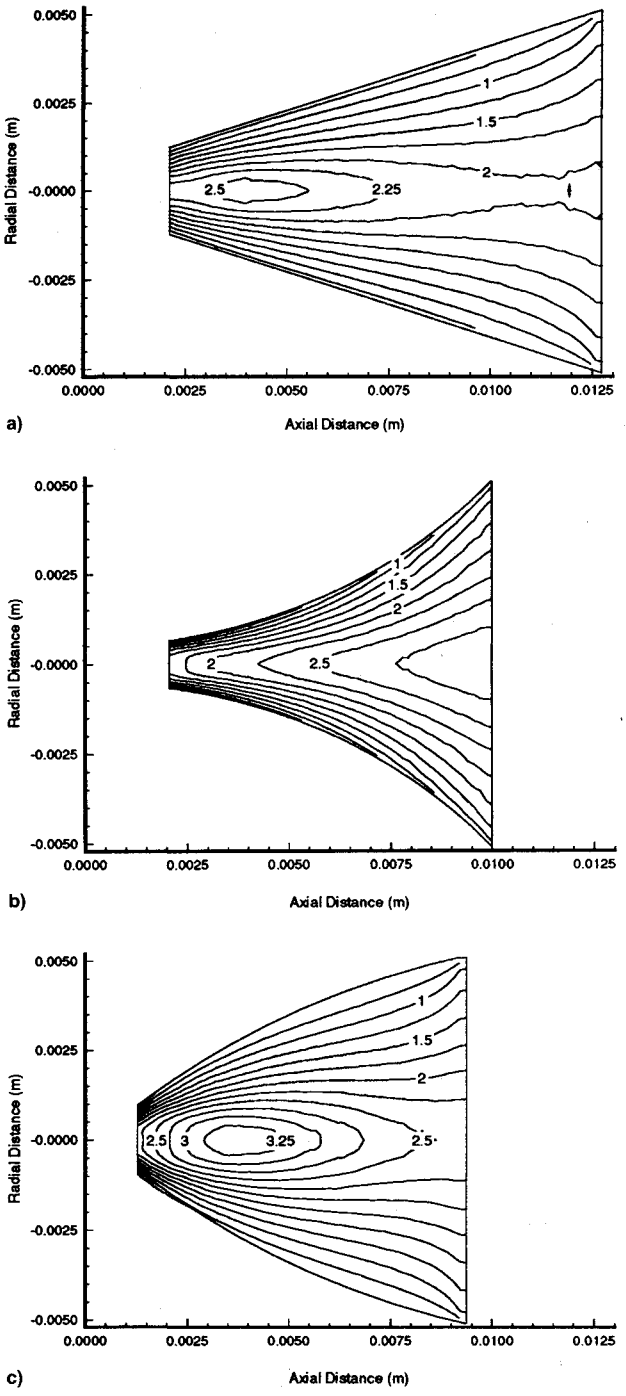

Fig. 6 Mach number contours of heated flow: a) cone, b) trumpet, and c) bell.

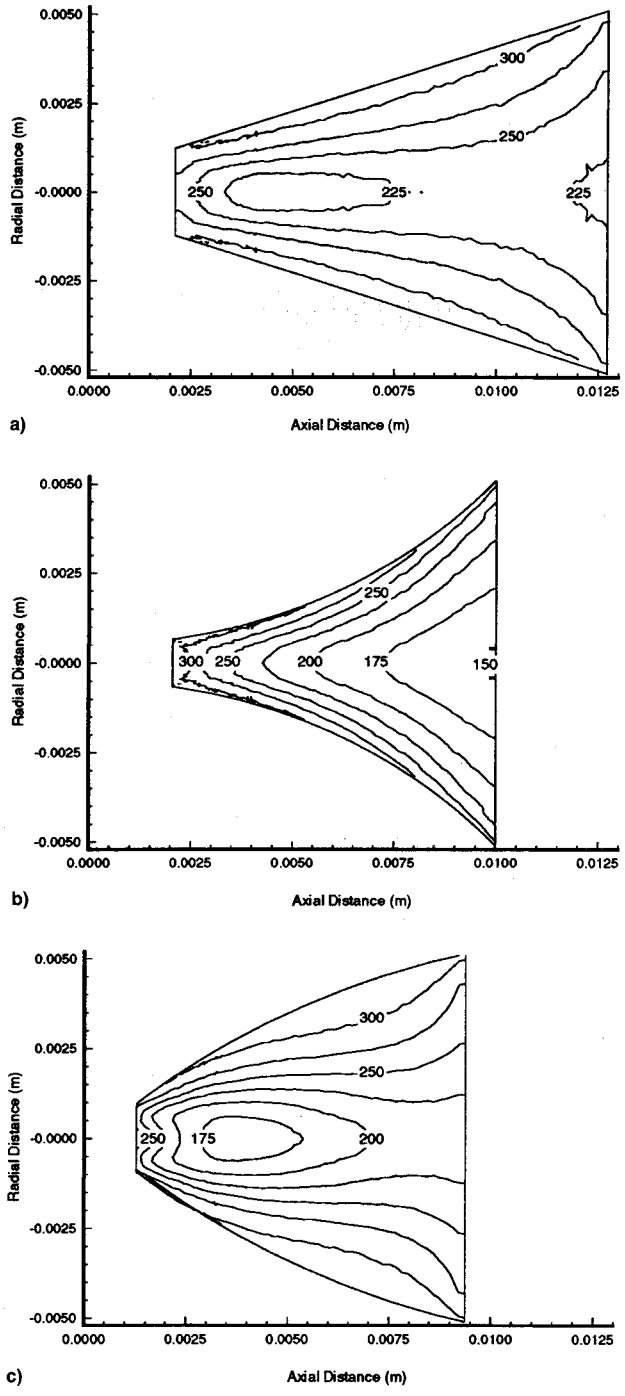

Fig. 7 Temperature contours of heated flow (K): a) cone, b) trumpet, and c) bell.

tinuously down the axis, while the gas temperature increases in the other two nozzles. In both the bell-shaped and conical nozzles, a "pocket" of cooler flow forms in the center of the diffuser where the gas expands to a minimum temperature. Upstream from the exit the viscous layer grows to a point where it fills the entire nozzle and the gas temperature increases, reducing thrust.

In order to compare the overall performance of each nozzle, specific characteristics are calculated and summarized in Table 1. The thrust, specific impulse, efficiency and discharge coefficient of each nozzle are compared. The ideal specific impulse for nitrogen in this case is 76.6 s. The ideal mass flow rates for each nozzle are included in the table because they are different for each geometry, as explained earlier in this section.

The conical nozzle produces the greatest amount of thrust because it sustains the highest mass flow rate; however, it has the lowest efficiency of all three nozzles. The trumpet has the highest efficiency of 83%, which is 5% greater than the cone. The cone has the highest discharge coefficient of 0.92, which is 12% higher than the trumpet and 7% higher than the bell. The trumpet more efficiently expands the flow because it has a thinner wall viscous layer, but its throat boundary layer is very thick, which constricts the flow at the throat. The cone performs best at the throat, but because the wall viscous layer grows thick in the diffuser, the flow is unable to expand to its potential anywhere inside the nozzle. The bell has a thinner throat boundary layer than the trumpet also, thus allowing the greatest expansion initially, but its wall contour causes the most viscous losses and the flow temperature increases downstream, negating the high performance at the throat.

Heated Flow Results

In this section, the results from the heated flow simulations are presented and compared. Figure 6 compares the Mach

Table 1 Performance characteristics of unheated nozzle flow

Performance characteristic	Cone	Trumpet	Bell
Thrust, $N \times 10^{-4}$	9.63	9.32	9.30
I_{sp}, s	60.6	63.6	61.6
η_{isp}, %	79	83	80
$\dot{m}_{ideal}$, mg/s	1.75	1.82	1.78
$\dot{m}_{actual}$, mg/s	1.62	1.50	1.54
C_D	0.92	0.82	0.86

Table 2 Performance characteristics of heated nozzle flow

Performance characteristic	Cone	Trumpet	Bell
Thrust, $N \times 10^{-4}$	7.75	7.74	7.94
I_{sp}, s	64.5	68.4	68.9
η_{isp}, %	46	49	49
$\dot{m}_{ideal}$, mg/s	1.34	1.41	1.38
$\dot{m}_{actual}$, mg/s	1.23	1.15	1.17
C_D	0.92	0.82	0.85

number contours plotted for each nozzle configuration. The contours are very similar to those of the unheated flow simulations. The bell expands the flow to a higher Mach number, but the viscous layer fills the entire nozzle by the time the flow reaches the exit plane. The trumpet flow expands the flow the most uniformly and has a higher average Mach number at the exit plane.

Figure 7 is a comparison of temperature contour plots of all three nozzles. In the conical nozzle, the flow enters the computational flow region with an almost uniform temperature between 250–300 K, except near the wall, where the flow is above 300 K. Because the wall is at a constant 293 K, heating due to viscous dissipation occurs at the wall. The temperature decreases as the flow expands, but it is only able to decrease to values above 200 K due to heating in the viscous layer. The flow enters the trumpet-shaped computational area at essentially a uniform temperature above 300 K, but the temperature decreases to values between 150–200 K at the exit, and even decreases to 100 K in the plume. The temperature in the bell-shaped nozzle decreases initially to under 150 K, but a great deal of heating occurs in the viscous layer, evidenced by the large area near the wall which has temperatures greater than 300 K. The flow becomes warmer as the flow advances towards the exit plane.

The performance characteristics of the nozzles with heated flow are summarized in Table 2. The ideal specific impulse for heated nitrogen flow is 140 s, based on a stagnation temperature of 1000 K. The most significant characteristic to note is the efficiency, which drops to below 50% for all three nozzles. This is explained by the fact that the ideal specific impulse is calculated based on a constant stagnation temperature of 1000 K, which would be the case for one-dimensional, isentropic flow. In reality, a great deal of the flow heat is transferred to the wall, which is at a temperature of 293 K. The stagnation temperature drops significantly as the flow travels through the nozzle, and a great deal of energy is lost to the wall. The thrust that is produced is not nearly as high as it could have been. In both experimental tests and actual thruster performance, the nozzle wall heats up and not nearly as much energy is lost through heat transfer. Both the trumpet and bell-shaped nozzles are more efficient than the cone by about 6.5%, with the bell producing the most thrust. The discharge coefficients for the heated flow are almost identical to those for the unheated flow, which indicates that flow temperature has no effect on throat boundary-layer growth.

The reason that less thrust is produced with the heated flow than with the flow at room temperature is that in order to keep the initial stagnation pressures equal in both cases, the mass flow rate is decreased in the heated flows. This decreases the amount of thrust that can be produced. The average throat Reynolds number in the unheated flow cases is 117, while in the heated flow cases it is 90, so there is not a significant difference in Reynolds numbers for all of the cases.

Nozzle Throat Configuration

Several studies have examined the effects of nozzle throat configuration on discharge coefficient.[6,8,22–26] Throat radius of curvature seemed to be the significant parameter in each study. Back et al.[22] found that a decrease in throat radius of curvature resulted in a decrease in discharge coefficient, but he only measured flows at higher Reynolds numbers (10^6). Whalen[6] experimented with low Reynolds number flows (<6000) through nozzles of various contours and found the opposite trend: an increase in throat radius of curvature resulted in a decrease in discharge coefficient. A significant difference between the two studies mentioned besides the flow Reynolds number was that in Back's investigation the throat radius of curvature was constant. In Whalen's study, the outlet radius of curvature was different from the inlet radius of curvature in each case, but the inlet radius of curvature was constant among all geometries. The geometric conditions used for the present study are similar to those in Whalen's study, where the inlet radius of curvature is constant for all cases, but the outlet radius of curvature differs for each geometry. For comparison, each outlet radius of curvature is normalized by the throat radius, and is equal to 1 for the conical nozzle, 4 for the bell, and 26 for the trumpet. The trend in the flow simulations is for an increase in nozzle discharge coefficient with a decrease in throat radius of curvature, which is the same trend found by Whalen. The trumpet has the lowest discharge coefficient of 0.82, the bell has a discharge coefficient of 0.85, and the cone has the highest of 0.92. The flow in the nozzle throat area has a significant effect on the flow throughout the nozzle. More work needs to be done in the study of nozzle throat flow phenomena in order to better predict nozzle performance and keep losses to a minimum.

Conclusions

Low-density nitrogen flows through three nozzles with different wall contours are simulated with DSMC in order to investigate the effects of geometry on nozzle performance. Large viscous layers exist at the low Reynolds numbers at which these nozzles operate, with little or no isentropic core flow present. Flow simulations are performed with an unheated gas in order to separate the heat-transfer losses present in hot gas flow from the flow divergence losses and viscous losses that occur in all of the flows. The trumpet-shaped nozzle is the most efficient of the three nozzle geometries. It has a 5% higher efficiency than the cone, and nearly a 4% higher efficiency than the bell. A 5% increase in specific impulse efficiency would provide a 10% increase in thrust power per thruster in an electrothermal propulsion system, which would amount to a substantial payback for a system consisting of many thrusters.[1] The trumpet and bell-shaped nozzles have the same efficiency with the heated flow, which is 6.5% higher than the conical nozzle efficiency. Although the trumpet has the lowest discharge coefficient, it still performs the most efficiently. Both the cone and the bell have significantly larger viscous layers than the trumpet. The bell is able to expand the flow to higher Mach numbers than the other two nozzles, but its viscous layer grows to fill the entire diffuser and decelerates the flow towards the exit plane. The question remains whether or not the bell-shaped nozzle's efficiency would continue to improve compared to the trumpet's efficiency with an increase in stagnation temperature.

The effects of the increased stagnation temperature are significant in all three nozzle geometries. The flows exhibit a large increase in nonisentropic flow losses, including viscous effects and heat-transfer effects. It can be concluded that the increase in stagnation temperature increases the viscous effects and losses which occur in low Reynolds number nozzle flows.

Acknowledgments

The authors would like to thank S. Venkateswaran and Hsin-Hua Tsuei for their assistance with the continuum code investigation.

References

[1]Grisnik, S. P., and Smith, T. A., "Experimental Study of Low Reynolds Number Nozzles," AIAA Paper 87-0992, May 1987.

[2]Murch, C. K., Broadwell, J. E., Silver, A. H., and Marcisz, T. J., "Performance Losses in Low-Reynolds-Number Nozzles," AIAA Paper 68-91, Jan. 1968.

[3]Brophy, J. R., Pivirotto, T. J., and King, D. Q., "Investigation of Arcjet Nozzle Performance," AIAA Paper 85-2016, Oct. 1985.

[4]Rothe, D. E., "Electron-Beam Studies of Viscous Flow in Supersonic Nozzles," *AIAA Journal*, Vol. 9, No. 5, 1971, pp. 804–811.

[5]Penko, P. F., Boyd, I. D., Meissner, D. L., and Dewitt, K. J., "Pressure Measurements in a Low-Density Nozzle Plume for Code Verification," AIAA Paper 91-2110, June 1991.

[6]Whalen, M. V., "Low Reynolds Number Nozzle Flow Study," NASA TM-100130, July 1987.

[7]Hueser, J. E., Melfi, L. T., Jr., Bird, G. A., and Brock, F. J., "Analysis of Large Solid Propellant Rocket Engine Exhaust Plumes Using the Direct Simulation Monte Carlo Method," AIAA Paper 84-0496, Jan. 1984.

[8]Kuluva, N. M., and Hosack, G. A., "Supersonic Nozzle Discharge Coefficients at Low Reynolds Numbers," *AIAA Journal*, Vol. 9, No. 9, 1971, pp. 1876–1879.

[9]Bird, G. A., *Molecular Gas Dynamics*, Oxford Univ. Press, London, 1976.

[10]Campbell, D. H., "DSMC Analysis of Plume-Freestream Interactions and Comparisons of Plume Flowfield Predictions with Experimental Measurements," AIAA Paper 91-1362, June 1991.

[11]Ratterni, L., Jr., "Bipropellant Engine Plume Analyses for the Mars Observer Scientific Spacecraft," AIAA Paper 90-1847, July 1990.

[12]Nelson, D. A., and Doo, Y. C., "Simulation of Multicomponent Nozzle Flows into a Vacuum," *Rarefied Gas Dynamics*, Vol. 116, Progress in Astronautics and Aeronautics, AIAA, Washington, DC, 1989, pp. 340–351.

[13]Boyd, I. D., and Stark, J. P. W., "Modeling of Small Hydrazine Thruster Plumes Using Discrete Particle and Continuum Methods," AIAA Paper 88-2631, June 1988.

[14]Boyd, I. D., Penko, P. F., and Carney, L. M., "Efficient Monte Carlo Simulation of Rarefied Flow in a Small Nozzle," AIAA Paper 90-1693, June 1990.

[15]Bird, G. A., "Monte Carlo Simulation in an Engineering Context," *Rarefied Gas Dynamics*, Vol. 74, Pt. I, Progress in Astronautics and Aeronautics, AIAA, New York, 1981, pp. 239–255.

[16]Borgnakke, C., and Larsen, P. S., "Statistical Collision Model for Monte Carlo Simulations of Polyatomic Gas Mixture," *Journal of Computational Physics*, Vol. 18, No. 4, 1975, pp. 405–420.

[17]Bird, G. A., "Perception of Numerical Methods in Rarefied Gas Dynamics," *Rarefied Gas Dynamics*, Vol. 118, Progress in Astronautics and Aeronautics, AIAA, Washington, DC, 1989, pp. 211–226.

[18]Choi, Y., and Merkle, C. L., "Time-Derivative Preconditioning for Viscous Flows," AIAA Paper 91-1652, June 1991.

[19]Venkateswaran, S., Weiss, J. M., Merkle, C. L., and Choi, Y., "Propulsion-Related Flowfields Using the Preconditioned Navier-Stokes Equations," AIAA Paper 92-3437, July 1992.

[20]Boyd, I. D., Penko, P. F., and Meissner, D. L., "Numerical and Experimental Investigations of Rarefied Nozzle and Plume Flows of Nitrogen," AIAA Paper 91-1363, June 1991.

[21]Zelesnik, D., "A Numerical Investigation of Low Reynolds Number Nozzle Flows by Use of the Direct Simulation Monte Carlo Method," M.S. Thesis, Pennsylvania State Univ., University Park, PA, 1992.

[22]Back, L. H., Massier, P. F., and Gier, H. L., "Comparison of Measured and Predicted Flows Through Conical Supersonic Nozzles, with Emphasis on the Transonic Region," *AIAA Journal*, Vol. 3, No. 9, 1965, pp. 1606–1614.

[23]Back, L. H., Cuffel, R. F., and Massier, P. F., "Influence of Contraction Section Shape and Inlet Flow Direction on Supersonic Nozzle Flow and Performance," *Journal of Spacecraft and Rockets*, Vol. 9, No. 6, 1972, pp. 420–427.

[24]Campbell, C. E., and Farley, J. M., "Performance of Several Conical Convergent-Divergent Rocket-Type Exhaust Nozzles," NASA TN-D-467, Sept. 1960.

[25]Cuffel, R. F., Back, L. H., and Massier, P. F., "Transonic Flowfield in a Supersonic Nozzle with Small Throat Radius of Curvature," *AIAA Journal*, Vol. 7, No. 7, 1969, pp. 1364–1366.

[26]Hopkins, D. F., and Hill, D. E., "Effect of Small Radius of Curvature on Transonic Flow in Axisymmetric Nozzles," *AIAA Journal*, Vol. 4, No. 8, 1966, pp. 1337–1343.